01,05

Multiferroic materials for Spintronics

© Z.V. Gareeva[1], V.V. Filippova[1], A.K. Zvezdin[2]

[1] Institute of Molecule and Crystal Physics, Subdivision of the Ufa Federal Research Centre of the Russian Academy of Sciences, Ufa, Russia
[2] Prokhorov Institute of General Physics, Russian Academy of Sciences, Moscow, Russia

E-mail: zukhragzv@yandex.ru

Received April 18, 2024
Revised April 18, 2024
Accepted May 8, 2024

The principal aspects of the operation of multiferroics-based spintronic devices; micromagnetic methods that allow modeling magnetoelectric and spin-orbit devices, as well as calculating the main parameters of multiferroic heterostructures have been discussed. The results of calculations of micromagnetic configurations realized in an electric field in heterostructures of ferromagnetic−multiferroics-type are presented, and the influence of sample dimensions on the magnetic states in the system is studied.

Keywords: multiferroics, magnetoelectric effect, bismuth ferrite, exchange bias effect.

DOI: 10.61011/PSS.2024.08.59036.22HH

1. Introduction

Oxide multiferroics are promising materials for energy-saving and highly efficient IT solutions involving the development of logical magnetoelectric devices that serve as basic hardware components of a new generation of computing microelectronics (microprocessors) based on novel physical and technological principles [1].

The use of magnetic and magnetoelectric materials in spintronics is of great interest. This interest arises from the possibility of preserving data recorded on magnetic media in the case of power interruptions, implementing power-saving modes through the use of magnetic and magnetoelectric materials (upon capacitor recharging), miniaturizing electronic devices, applying spin currents, which have a wider range of properties than electrical ones, and controlling them by means of various stimuli, such as electrical currents, low-magnitude magnetic fields, and electrical fields, which may be produced in multiferroic materials.

One of the latest designs of an advanced magnetoelectric spin-orbit (MESO) transistor [1] developed at Intel based on materials with magnetoelectric interaction and materials with strong spin-orbit coupling is of the utmost interest in this context. Their combination provides a significant enhancement of technical parameters: an increase in switching speed of the device and a substantial reduction in power consumption.

At the present stage, the refinement of physical principles and methods of mathematical modeling of MESO devices; the selection of materials with optimum characteristics (high magnetoelectric coupling coefficients, low control voltages, small Hall angles, and high (near-room) operating temperatures) and techniques for adequate modeling of magnetic state switching processes; and the search for scaling and miniaturization approaches to production of compact circuits are essential for technological development.

The following aspects are discussed below: the main components and principles of operation of MESO devices; the mechanisms of magnetoelectric interactions in heterostructures based on multiferroics; the development of a technique for modeling of magnetic state switching processes in the systems under consideration; and the calculation of micromagnetic structures in nanoelements based on ferromagnetic−multiferroic structures that may be used in advanced spintronic logic devices.

2. Magnetoelectric materials for MESO devices

2.1. Principle of operation and structure of MESO elements

The MESO technology proposed in [1–4] is a logical evolution of the MRAM concept, which has gone through several stages in its development, including two generations of commercial MRAM with switching of magnetization of a magnetoresistive element under the influence of a magnetic field (toggle MRAM) and spin-polarized currents (STT-MRAM), to the PIM (processing-in-memory) concept associated with architectures that allow one to use a memory cell for calculations and data processing. Technologies related to the development of near-memory processing and in-memory processing architectures have been discussed in detail in literature [5]. In what follows, we focus on a MESO device that may be used to store data and perform logical operations.

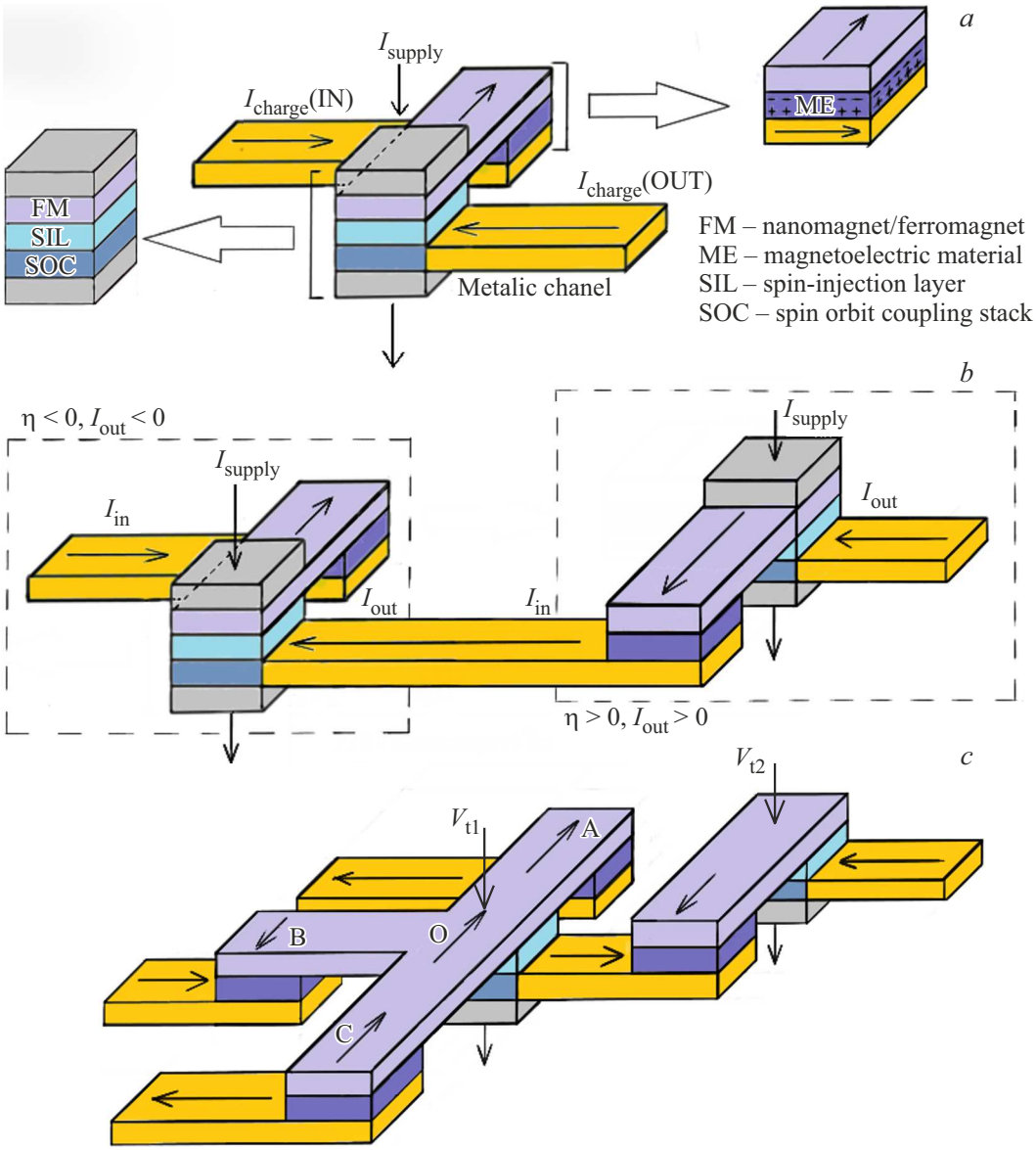

Figure 1. *a*) Diagram of a MESO device; *b*) logic gate; *c*) cascade [6].

Schematic diagrams of MESO devices are shown in Figure 1. The main MESO components are a nano-sized ferromagnet (nanomagnet), which undergoes magnetization switching, and the associated magnetoelectric (ME) and spin-orbit (SO) components (Figure 1, *a*). A bit line is connected to the ME component to supply an input electrical signal that produces an electric field at the ME element, which serves as an ME capacitor. A change in polarization of the multiferroic under the influence of the electric field of current leads to switching of the magnetic state of the nanomagnet (due mostly to the bias effect induced in the case of exchange coupling between the ferromagnet and the multiferroic in the ME component). To read out the new magnetic state, supply current is applied to the SO component. This current becomes spin-polarized when passing through the ferromagnetic layer, and the spin polarization depends on the current magnetic state of the nanomagnet. Flowing further through the injection layer, the spin-polarized current enters a material with a strong spin-orbit interaction, which drives the conversion of spin into charge, and electric current with its direction determined by the polarization of electron spins is supplied to the output bit line. In this design, input and output currents are directed opposite to each other, allowing one to use the MESO element as a logic gate (Figure 1, *b*). The high efficiency of spin-to-charge conversion, which is ensured by the use of materials with strong SO coupling, contributes to the generation of an output current with a sufficiently high density, which provides an opportunity to construct cascade circuits from several MESO elements (Figure 1, *c*). The output current of one MESO element is used as the input current of another, enabling data transmission and allowing

one to perform Boolean operations in cascades of three or more elements. According to the estimates from [1–4], devices of this kind are characterized by a high logic element density and reduced response delays, which results in a high computing performance; magnetic states are switched within time intervals on the order of 10^{-9} s; the energy required for switching is of the order of fJ/bit; and voltages are reduced to 0.3 V, making the study of opportunities for development of this technology attractive for researchers and technologists.

2.2. Magnetoelectric heterostructures

In the context of spintronic logic devices, the study of multiferroic systems is focused on magnetoelectric heterostructures, since magnetic–multiferroic systems are used directly in the MESO design and magnetoelectric coupling coefficient α_{MC} may be increased by introducing a ferromagnetic/antiferromagnetic layer. The magnitudes of magnetoelectric coupling coefficients for single crystals and composite structures based on multiferroics are listed in the table for comparison. The values of these parameters for various multiferroic structures were also reported in [7,8]. It can be seen that magnetoelectric heterostructures have significantly higher α_{ME} values than single-phase multiferroics.

Note that a wide variety of multiferroic heterostructures have already been designed. They may be classified, e.g., by the nature of magnetoelectric (ME) coupling in the interface region, which may take the form of a direct exchange interaction; an indirect Dzyaloshinskii–Moriya interaction; or a magnetoelastic interaction caused by „strain“ effects (mechanical stresses in the interface region) and chemical processes associated with the ionization and migration of oxygen anions and a change in the density of electron states (DOS) in the interface region [10]. In the third case, the electric field alters the electronic structure of the interface, inducing a change in saturation magnetization, magnetic anisotropy constants, and interlayer exchange interaction, which affect magnetoelectric effects (MEEs) and spin reorientation processes. Examples of magnetoelectric structures supporting such interactions include (i) ferromagnetic–piezoelectric (with MEEs caused by mechanical stresses and striction effects); (ii) antiferromagnetic–piezoelectric (with MEEs arising due to exchange striction caused by mechanical stresses); (iii) ferromagnetic–multiferroic (with MEEs associated with exchange interactions in the interface region); and (iv) multiferroic–piezoelectric structures, where MEEs may be tied to piezoelectric effects and the Dzyaloshinskii–Moriya interaction. It follows from the table that the magnetoelectric coupling coefficients may be fairly high in heterostructures with different mechanisms of ME interactions.

3. Modeling of spin reorientation processes in ferromagnetic–multiferroic films

Let us investigate a ferromagnetic–multiferroic ($CoFe/BiFeO_3$) structure with exchange interlayer interaction that was used in a MESO prototype in [2]. The advantages of using this system as a model object of study include the availability of fairly reliable data on the magnetoelectric properties of $BiFeO_3$ [9–15] and experimental data on magnetization reversal processes in $CoFe/BiFeO_3$ films [13], which may be used to verify the results of theoretical research.

Note that micromagnetic modeling packages (OOMMF, SPIN PM, MuMax, etc.) used for the analysis of micromagnetic structures in confined systems (films, nanoelements, multilayer structures) are focused on ferromagnetic materials. In view of this, an approach combining micromagnetic simulation methods and calculations based on the Ginzburg–Landau theory is fitting for calculation of magnetic states in a ferromagnetic–multiferroic system. If antiferromagnetic ordering is established in a multiferroic (as is the case with $BiFeO_3$), unidirectional magnetic anisotropy (UMA) is induced in the interface region of the ferromagnetic–multiferroic structure. The orientation of the easy UMA axis is correlated with the direction of the antiferromagnetic vector of the multiferroic. Exchange bias effects, which consist in a shift of the hysteresis dependence of the ferromagnet magnetization ($M_F(H)$) along the horizontal axis ($\mathbf{H}$), are observed in ferromagnetic–antiferromagnetic systems. The ferromagnetic layer thickness should not exceed $t_{\mathrm{FM}} = \pi\sqrt{A_F/K_F}$ in this case; this condition is needed for continuous reorientation of spins at the interface and to avoid the emergence of spin-uncoupled regions. According to the estimates presented in [14], the magnitude of the exchange bias field is $H_{eb} = -J_{eb}/\mu_0 M_F t_F$, where $J_{eb} = A_{af}/S$ is the exchange coupling constant defined as the ratio of the exchange interaction constant of the antiferromagnet to its surface (S) and M_F is the saturation magnetization of the ferromagnet. Thus, magnetic ordering with the magnetization oriented parallel to antiferromagnetic vector $\mathbf{L} = (\mathbf{M}_1 - \mathbf{M}_2)/2M_0$, where $\mathbf{M}_{1,2}$ are the magnetizations of sublattices of the multiferroic and M_0 is the saturation magnetization, is established in the thin ($t < t_{\mathrm{FM}}$) ferromagnetic layer (pinning layer) due to the exchange interaction with the antiferromagnetic multiferroic. The schematic diagram of the system is shown in Figure 2.

Within this model, the free energy of the system includes the ferromagnetic layer energy, the multiferroic energy, and the energy of the interface pinning layer

$$F(\mathbf{M}_{\mathrm{FM}}, \mathbf{P}, M_{MF}, \mathbf{L}) = F_{\mathrm{FM}}^{soft}(\mathbf{M}_{\mathrm{FM}}^{soft}) + F_{\mathrm{FM}}^{pinning}(\mathbf{M}_{\mathrm{FM}}^{pinning}) + F_{MF}(\mathbf{P}, \mathbf{M}_{MF}, \mathbf{L}), \quad (1)$$

Magnetoelectric coupling coefficients for multiferroic systems

Multiferroics	α	Temperature, K	Reference
$BiFeO_3$	4.2 V/cm · Oe	300	[9]
$GdFe_{0.94}Mg_{0.06}O_3$	1.67 V/cm · Oe	400	[7]
$CoFe_2O_4/BaTiO_3$	8.1 mV/cm · Oe	300	[7]
$BiFeO_3/BaTiO_3$	24 V/cm · Oe	300	[9,10]
α-Fe_2O_3/PZT	4.8 V/(Oe · cm)	300	[11]
$SrTiO_3/BaTiO_3$	495 mV/cm · Oe	200	[12]

where the ferromagnetic layer energy is given by

$$F_{\mathrm{FM}}^{soft}\left(\mathbf{M}_{\mathrm{FM}}^{soft}\right) = A_{\mathrm{FM}}\left(\nabla \mathbf{m}_{\mathrm{FM}}^{soft}\right)^2 + K_{cub}\left(\left(m_{\mathrm{FM}_x}^{soft}\right)^2 + \left(m_{\mathrm{FM}_y}^{soft}\right)^2 + \left(m_{\mathrm{FM}_z}^{s} oft\right)^2\right) + K_u\left(\mathbf{n}_u \mathbf{m}_{\mathrm{FM}}^{soft}\right)^2, \quad (2)$$

the pinning layer energy is

$$F_{\mathrm{FM}}^{pinning}\left(\mathbf{m}_{\mathrm{FM}}\right) = K_u^{pinning}\left(\mathbf{n}_u m_{\mathrm{FM}}^{hard}\right)^2 - M_{\mathrm{FM}}^{hard}\left(\mathbf{H}\cdot\mathbf{m}_{\mathrm{FM}}^{hard}\right), \quad (3)$$

and the multiferroic energy is

$$F_{MF}\left(\mathbf{P}, \mathbf{M}_{MF}, \mathbf{L}\right) = F_{me}\left(\mathbf{M}_{MF}, \mathbf{L}, \mathbf{P}\right) + F_{el}\left(\mathbf{P}, \mathbf{E}\right), \quad (4)$$

where the ferroelectric and magnetoelectric components are

$$F_{el}\left(\mathbf{P}, \mathbf{E}\right) = -\mathbf{P}\cdot\mathbf{E} + a_0\frac{P_z^2}{2} + a_1\frac{P_z^4}{4} + \ldots \quad (5)$$

$$F_{me}\left(\mathbf{M}_{MF}, \mathbf{L}, \mathbf{P}\right) = \frac{1}{2\chi_\perp}M_0^2\mathbf{m}_{MF}^2 + \frac{\chi_\perp}{2}\left(\mathbf{D}\cdot\left[\mathbf{L}\times\mathbf{m}_{MF}\right]\right) + A(\nabla L)^2 + \gamma\mathbf{e}_p\left(\left(\mathrm{grad}\,\mathbf{L}\right)\cdot\mathbf{L} - \mathbf{L}\cdot\left(\mathrm{grad}\,\mathbf{L}\right)\right) + K_1\left(\mathbf{n}_u\mathbf{L}\right)^2, \quad (6)$$

where A_{FM} is the exchange interaction constant, K_{cub} is the cubic magnetic anisotropy constant, K_u is the uniaxial magnetic anisotropy constant, and γ is the inhomogeneous magnetoelectric interaction parameter.

It is known that the inhomogeneous magnetoelectric interaction in the $BiFeO_3$ multiferroic stabilizes the antiferromagnetic cycloid, which is the ground magnetic state of $BiFeO_3$ single crystals [15]. However, mechanical stresses induced by the substrate in $BiFeO_3$ films may disrupt the cycloid phase and trigger the formation of a homogeneous state with a given orientation of vector **L**. Experimental data on the ground magnetic states in $BiFeO_3$ films grown on various ferroelectric substrates and theoretical research data, which allow one to determine the stability regions of spin cycloids and homogeneous magnetic states, were presented in [16–19].

Let us consider the range of material parameters that establish homogeneous antiferromagnetic ordering in a multiferroic film. Calculations carried out using the Ginzburg–Landau theory for energy (6) provide an opportunity to determine the ground states of the multiferroic (orientation of weak ferromagnetism **M** and antiferromagnetism **L** vectors) and their transformation under the influence of

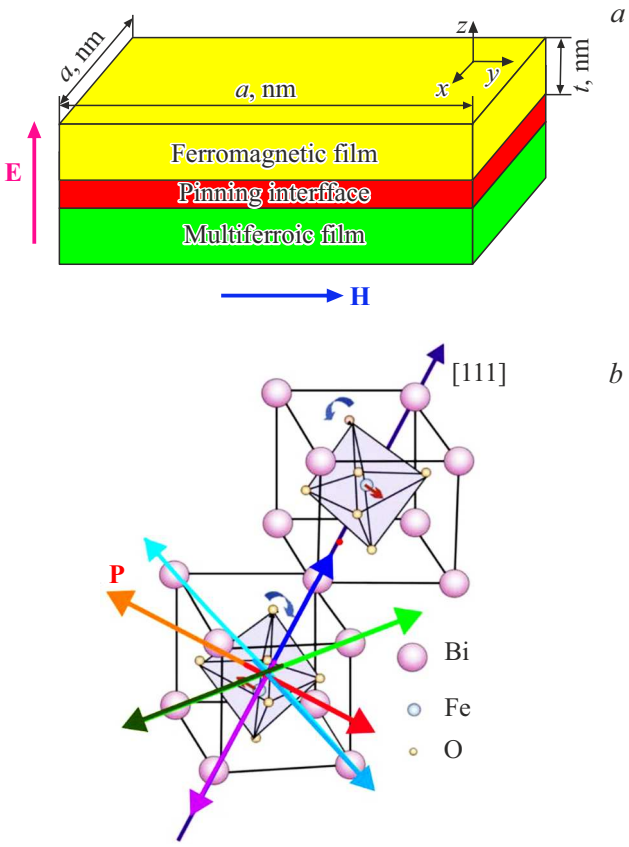

Figure 2. *a*) Schematic diagram of the system; *b*) unit cell of $BiFeO_3$.

an electric field [20,21]. Assuming that the direction of antiferromagnetic vector **L** determines the UMA axis orientation in the pinning layer, we consider an exchange-coupled ferromagnetic structure consisting of a layer of a soft magnetic ferromagnet and a ferromagnetic pinning layer with a preferred UMA direction. Micromagnetic structures in a system of this kind may be analyzed via micromagnetic modeling in OOMMF, which allows one to determine the equilibrium magnetic configurations in a ferromagnetic film at a given direction of the electric field. Let us use the following parameters: the film size is $a \times a \times t\,\mathrm{nm}^3$, the cell size is $5 \times 5 \times 3\,\mathrm{nm}^3$, $a = 200\,\mathrm{nm}$, $t = n \cdot 20/,\mathrm{nm}$, t is the ferromagnetic layer thickness, a denotes the transverse dimensions of the nanoelement, the pinning layer thickness

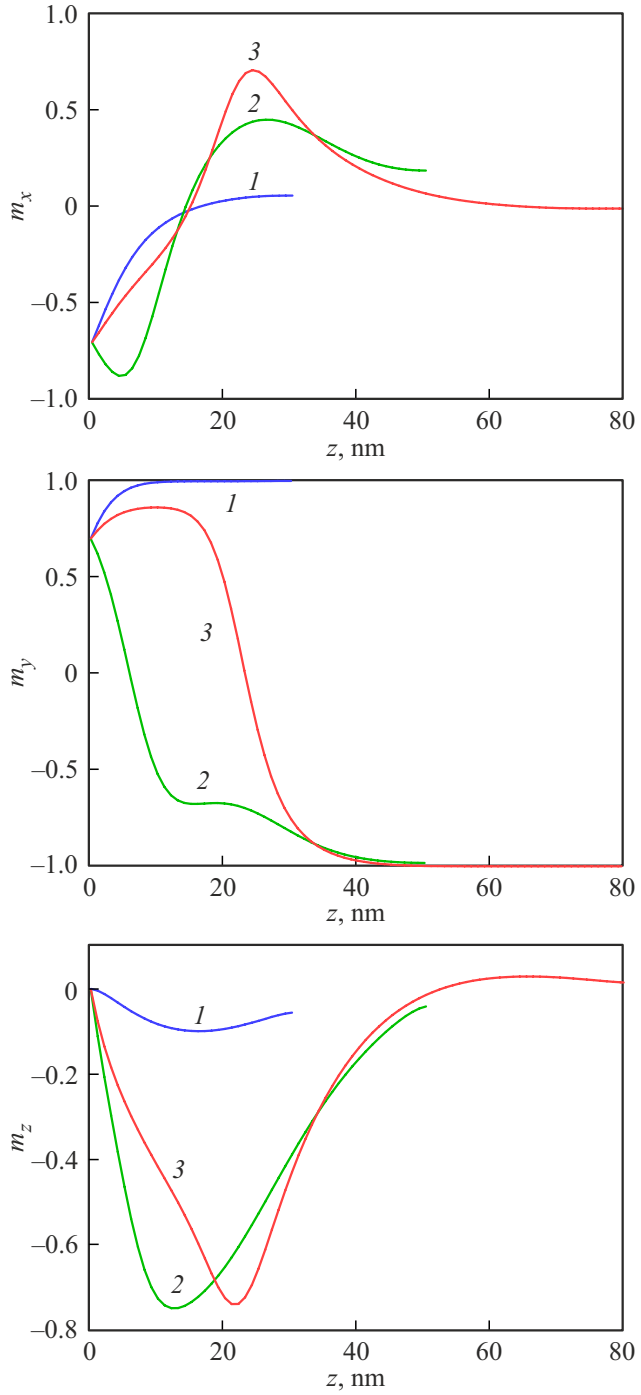

Figure 3. Dependences of the magnetization vector components on coordinate z along the sample thickness. Curve *1* corresponds to $a = 30$ nm; curve *2*, to $a = 50$ nm; curve *3*, to $a = 80$ nm.

is 1 nm, $K_{pinning} = -1 \cdot 10^4$ J/m^3, and the magnetic parameters of the ferromagnetic layer correspond to the parameters of iron garnets ($A = 3 \cdot 10^{-12}$ J/m^2, $K_{cub} = 1 \cdot 10^7$ J/m^3, $K_u = -1 \cdot 10^4$ J/m^3).

We assume that the electric polarization vector in the multiferroic is oriented in preferred direction $\mathbf{P}_0$ in zero magnetic field. Vectors $\mathbf{M}_0$ and $\mathbf{L}_0$ corresponding to this direction are determined from the minimum of energy (6). The electric field induces reorientation of vector $\mathbf{P}_f$ and, consequently, vectors $\mathbf{M}_f$ and $\mathbf{L}_f$. Data on the mutual orientation of vectors $\mathbf{P}, \mathbf{M}$ and $\mathbf{L}$ in $BiFeO_3$ films for different plates and stretching and compression strains induced by the orienting substrate were reported in [21]. The results of calculation of magnetic configurations for $BiFeO_3$ films with crystallographic orientations (001), (110) were presented in [22,23]. Note that these calculations allow one to reproduce the effect of the hysteresis dependence shift at different polarization orientations in a multiferroic induced by an electric field. Thus, the above model provides an opportunity to investigate the processes of spin reorientation in a ferromagnetic–multiferroic structure and examine the influence of various factors on magnetic states in the system. Let us focus on the geometric factor associated with the sample size.

Moore's law imposes constraints on the physical size of transistors in integrated circuits. Certain patterns in respect to MESO transistors may also be observed. It was demonstrated in [1] that following ratio between input I_c and output $\mathbf{I}_s$ currents should be fulfilled to ensure efficient MESO operation:

$$I_c = \frac{1}{w} \lambda_{\mathrm{ISOC}} [\sigma \times \mathbf{I}_s], \tag{7}$$

where $\mathbf{I}_s$ is the input electric current ($\| OX$) to the ME element; w is the minimum device dimension (width); σ is the intrinsic magnetic moment vector of an electron defined by Pauli matrices; $\mathbf{I}_s$ is the spin current ($\| OZ$) at the output of the SO element; and λ_{ISOC} is the effective diffusion length of spin current. According to the estimates made in [1,6], nanomagnet dimensions w may be reduced approximately to 20–30 nm. Let us consider the magnetic states that may emerge in nanoelements when their size changes.

Figure 3 shows magnetization trajectories $\mathbf{m}(x)$ calculated within the above approach. It can be seen that nearly homogeneous magnetization distributions are established in the ferromagnetic layer at the chosen values of physical parameters and small dimensions of the nanoelement. However, with an increase in transverse dimensions of the nanoelement, inflection points emerge in the $m_i(x)$, $i = x, y, z$ dependences, indicating the possibility of formation of vortex-type topological structures that may be used in scaling of spintronic devices.

4. Conclusion

The key aspects of development of spintronics based on magnetoelectric materials were discussed using the example of a magnetoelectric spin-orbit transistor. Its structure and principles of operation were examined. Heterostructures based on the $BiFeO_3$ multiferroic were used as an example to develop a method of calculation of magnetic states in exchange-coupled ferromagnetic–multiferroic films with the exchange bias effect. This technique relies on the concept

of a ferromagnetic pinning layer with unidirectional magnetic anisotropy forming in the ferromagnetic–multiferroic interface region and allows one to use software packages for micromagnetic calculation (specifically, OOMMF) to calculate magnetic configurations and their transformations under the influence of magnetic and electric fields in confined films and nano-sized structures. Magnetic states in nanoelements of various sizes were calculated for a $CoFe/BiFeO_3$ system.

Funding

This study was supported by grant No. 23-22-00225 from the Russian Science Foundation.

Conflict of interest

The authors declare that they have no conflict of interest.

References

[1] S. Manipatruni, D.E. Nikonov, C.-C. Lin, T. A. Gosavi, H. Liu, B. Prasad, Y.-L. Huang, E. Bonturim, R. Ramesh, I.A. Young. Nature **565**, 7737 (2019).
[2] S. Manipatruni, D.E. Nikonov, I.A. Young. Nature Phys. **14**, 4 (2018).
[3] J. Zeng, N. Xu, Y. Chen, C. Huang, Z. Li, L. Fang. AIMCU-MESO: ACM Trans. Des. Autom. Electron. Syst. (2022).
[4] J. Zeng, P. Yi, B. Chen, C. Huang, X. Qi, S. Qiu, L. Fang. Microelectronics J. **116**, 105235 (2021).
[5] Z. Guo, J. Yin, Y. Bai, D. Zhu, K. Shi, G. Wang, K. Cao, W. Zhao. Proc. IEEE **109**, 1398 (2021).
[6] Z. Liang, M. Mankalale, J. Hu, Z. Zhao, J.-P. Wang, S. Sapatnekar. IEEE J. Explor. Solid State Comp. Dev. Circ. **PP**, 1 (2018).
[7] R. Gupta, R. K. Kotnala. J. Mater. Sci. **57**, 12710 (2022).
[8] C. A. F. Vaz ,U. Staub. J. Mater. Chem. C **1**, 6731 (2013).
[9] M. Lorenz, G. Wagner,V. Lazenka, P. Schwinkendorf, H. Modarresi, M.J. Van Bael, A. Vantomme, K. Temst, O. Oeckler, M. Grundmann. Appl. Phys. Lett. **106**, 012905 (2015).
[10] P.B. Meisenheimer, S. Novakov, N.M. Vu, J.T. Heron. J. Appl. Phys. **123**, 240901 (2018).
[11] D.A. Burdin, D.V. Chashin, N.A. Ekonomov, L.Y. Fetisov, V.L. Preobrazhensky, Y.K. Fetisov. Sensors **23**, 13 (2023).
[12] X. Liu , Wenjie Song, Mei Wu, Yuben Yang, Ying Yang et al. Nature Commun. **12**, 1 (2021)
[13] H. Niu, J.L. Bosse, Q. He, Y. Gao, M. Trassin et al. J. Am. Chem. Soc. **139**, 1520 (2017).
[14] W.H. Meiklejohn, C.P. Bean. Phys. Rev. **102**, 1413 (1956).
[15] I. Sosnowska, A.K. Zvezdin.J. Magn. Magn.Mater. **140**–**144**, 167 (1995).
[16] D.Sando, A. Agbelele, D. Rahmedov, J. Liu, P. Rovillain, C. Toulouse, I. C. Infante, A. P. Pyatakov, S. Fusil, E. Jacquet, C. Carr'et'ero, C. Deranlot, S. Lisenkov, D. Wang, J.-M. le Breton et al. Nature Mater. **12**, 641 (2013).
[17] Z.V. Gareeva, A.F. Popkov, S.V. Soloviov, A.K. Zvezdin. Phys. Rev. B **87**, 214413 (2013).
[18] N.E. Kulagin, A.F. Popkov, S.V. Solov'yov, A.K. Zvezdin. Phys. Solid State **61**, 108 (2019).
[19] N.E. Kulagin, A.F. Popkov, A.K. Zvezdin. Phys. Solid State **53**, 970 (2011).
[20] A.F. Popkov, N.E. Kulagin, S.V. Soloviov, K.S. Sukmanova, Z.V. Gareeva, A.K. Zvezdin. Phys. Rev. B **92**, 140414 (2015).
[21] A.A. Berzin, D.L. Vinokurov, A.I. Morozov. Phys. Solid State **58**, 2320 (2016).
[22] Z.V. Gareeva, N.V. Shulga, A.K. Zvezdin. J. Magn. Magn. Mater. **587**, 171323 (2023).
[23] Z. Gareeva, N. Shulga, R. Doroshenko, A. Zvezdin. Phys. Chem. Chem. Phys. **25**, 22380 (2023).

Translated by D.Safin